Gravity current escape from a topographic depression

Edward W. G. Skevington [1] and Andrew J. Hogg [2,*]
[1] *Energy and Environment Institute, University of Hull, Hull HU6 7RX, United Kingdom*
[2] *School of Mathematics, University of Bristol, Bristol BS8 1UG, United Kingdom*

(Received 24 March 2023; accepted 18 October 2023; published 9 January 2024)

An inertial gravity current released within a topographic depression may climb up the incline from a lower to an upper plateau if it is sufficiently energetic and then continue to flow unsteadily away from the step while simultaneously draining back into the depression. This density-driven motion is investigated theoretically using the shallow-water equations to simulate the flow up a smooth step from a lower to an upper horizontal plane and to compute the volume of fluid that escapes from the depression. It is shown that it is possible for all of the fluid to drain back down the step and that the volume of the escaped fluid diminishes with a power-law dependence on time. This phenomenon is explained by analyzing the unsteady flow of a gravity current along a semi-infinite horizontal plane along which the front advances but simultaneously fluid drains from the rear edge of the plane. The dynamics of this motion at early times is calculated both numerically and analytically. The latter exploits the hodograph transformation of the shallow water equation, a technique which allows rapid and precise evaluation of flow features such as reflections and the onset of bores. The flow at later times becomes self-similar, and the self-similarity is of the second kind. It features an anomalous exponent that provides the power-law dependence of the volume of fluid on time, and this exponent is a function of the imposed Froude number at the front of the current. In this way the diminishing volume of fluid that escapes from a topographic depression is explained quantitatively. Eventually the flow may transition to a regime in which drag becomes non-negligible; the model of simultaneous propagation and draining is extended to this regime to show that the escaped volume of fluid also decays temporally and ultimately vanishes.

DOI: 10.1103/PhysRevFluids.9.014802

I. INTRODUCTION

When dense fluid is released into a less-dense environment, gravitational forces can drive flow along a horizontal bed. These flows, usually termed gravity currents, occur in several environmental settings, including salinity-driven currents in estuaries, oceanic turbidity currents, and atmospheric dispersion of dense gas [1]. There is a rich scientific literature documenting their properties, including experimental studies, modeling, and direct numerical simulations [2].

Underlying topography exerts significant control over this density-driven motion (see, for example, Ref. [3]) and some recent studies have examined in detail how unsteady flows are

*a.j.hogg@bristol.ac.uk

affected by localized topography [4–6]. One extreme is when the current drains freely over an edge [7–9], while the other end member is when the current is fully reflected by an initially distant barrier [10]. In between are a range of behaviors in which the current partially overtops the barrier. For example, unsteady flows generated by instantaneous releases of relatively dense material may at first overtop the confining barrier, but some fluid is ultimately retained behind it [11].

This study tackles the interaction of a gravity current with topography in which the underlying bed rises smoothly from one horizontal plateau to another. Released dense fluid may be able to surmount the "step" and then continue to propagate along the elevated plateau while simultaneously draining back down the step. This type of motion arises following the release of dense material within a localized topographic depression, and the calculation of the ensuing density-driven propagation reveals ultimately how much of the dense material remains confined within the depression and how much escapes. Important dynamical features of this motion include the rise up the step, and the simultaneous propagation along it and draining from it. The combination of these effects, all driven by gravitational force associated with the density difference between the fluids, means that the motion is distinct from earlier studies of gravity currents that solely propagate along or drain from horizontal planes. In what follows we present results for flows generated from lock release conditions, which climb up, propagate along, and drain from a step. Furthermore, to draw out the interplay of latter phases of the unsteady motion, we also investigate the unsteady evolution of two-dimensional currents instantaneously released from a lock for which the fluid drains freely at one end and propagates with a distinct front at the other. We show that the dynamical features of this second problem are similar to the first class of flows up a step at sufficiently long times after release. This equivalence allows us to deduce a quasianalytical prediction of the volume of fluid that has escaped the topographic depression as a function of time.

Our study employs a shallow water model of gravity current motion, which is based on hydrostatic balance in the vertical due to streamwise lengths far exceeding the typical thickness of the flow (see, for example, Refs. [2,12]). The unsteady motion is initiated by instantaneous release from a lock. The rate of advance of the dense fluid is governed by an imposed dynamic condition, often termed the "Froude number condition" [13,14], while for the flows along a semi-infinite plane, the current drains freely at the edge of the plane [7,9]. We employ high-resolution numerical methods to integrate the partial differential equations that govern the motion, alongside analytical methods that capture various stages of the motion. In particular, the initial phases may be calculated using quasianalytical methods, exploiting the hyperbolic nature of the shallow water equations and extending the techniques of Ref. [15] and Ref. [16] to this new scenario. The later stages of the flow in which there is simultaneously propagation forwards and draining from the edge, progressively adjust to a self-similar state in which the coupling between the streamwise extent and the time following after release cannot be predicted solely on the basis of dimensional reasoning. Instead the state is a self-similar solution of the second kind [17]; the exponent underpinning the gearing between lengths and times is calculated as part of the solution and remains a function of the dimensionless parameters in the problem. Although several studies have identified self-similarity of the second kind for viscously dominated free-surface flows (e.g., Refs. [18,19]) and for flows in porous media (e.g., Ref. [20]), such self-similar states are relatively uncommon in the inviscid gravity current literature. Notably, Ref. [21] constructed a self-similar solution of the second kind for radially converging currents and Ref. [22] have shown that the long-time dynamics of an entraining gravity current also exhibit this form of self-similarity. Importantly for the inviscid problem analyzed in this contribution, we demonstrate that ultimately all of the gravity current may drain from the elevated plateau.

At much later times as the flows thin and slow, it is no longer appropriate to ignore the effects of drag and the motion transitions to a state in which the dominant balance of horizontal momentum is between the streamwise pressure gradient and basal drag (see Ref. [23] and Sec. V). On the assumption that the drag may be expressed as proportional to the square of the velocity field,

we derive the timescales at which this balance arises and construct a different self-similar state in this regime. At much later times when the current has slowed and thinned further so that viscous processes become dominant, the motion becomes a viscous gravity current that simultaneously advances and drains as modelled in Ref. [18] and Ref. [24]. In this scenario the linearity of the governing equation leads to the motion conserving the "dipole moment," rather than it volume (see Refs. [18,24] and Sec. V B for further details). We demonstrate how the self-similar solution of Ref. [18] fits in with our calculations.

Our contribution is structured as follows. We formulate the problem and introduce our methodologies in Sec. II. Then in Sec. III, we present numerical results of the flow of an instantaneously released gravity current up a smooth step onto an elevated plateau. In particular we calculate the temporal dependence of the volume of fluid that escapes from the topographic depression for different heights of the step to illustrate the dynamical processes and their interplay. In order to interpret these results, we then examine the inertia-dominated dynamics along a semi-infinite plane along which the current propagates and from which the fluid drains (Sec. IV). We first focus on the initial evolution and the temporal dependence of the draining flux (Sec. IV A) before analyzing the late-time dynamics, which we demonstrate are dependent on the value of the Froude number imposed at the propagating front of the flow, Fr (Sec. IV B). When $\mathrm{Fr} < 2$, we show that the entire propagating current adjusts to a self-similar state of the second kind, ultimately leading to all of the fluid draining from the step. Conversely when $\mathrm{Fr} \geqslant 2$, the bulk of the motion detaches from the edge of the step, leaving behind a thin flowing layer that connects via a shock to the rest of the flow. We show in Sec. IV C how to calculate quasianalytically the onset of the shock and that the upstream thin layer asymptotes to another self-similar state. Drag-affected dynamics on the plane are examined in Sec. V. Here we compute the motion on the assumption that it is governed by a balance between the streamwise pressure gradient and the drag, with fluid inertia having become negligible. Finally, we summarize in Sec. VI and demonstrate the applicability of our analysis to the motion of unsteady flow of dense fluid released instantaneously within a topographic depression (as reported in Sec. III). The paper also includes an Appendix, in which we document the hodograph transformation of the governing equations and the techniques that lead to the construction of the quasianalytical solutions; these analytical results, although appearing cumbersome, allow rapid and precise evaluation of the flow fields.

II. PROBLEM FORMULATION

We model the two-dimensional evolution of a gravity current released instantaneously from rest within a reservoir. The fluid propagates unidirectionally over a horizontal plane towards a smooth rise to an elevated horizontal plateau or in a second problem drains freely over a rearward edge (Fig. 1). The propagating fluid is of density $\rho(1+\Delta)$ and flows under the action of gravity through a deep environment of density ρ; the reduced gravity is given by $g' = \Delta g/(1+\Delta)$, where g denotes gravitational acceleration. The flow is along a semi-infinite surface of elevation $b(x)$ aligned with the x axis. In the first problem, the surface rises from one horizontal plane to another; the latter is elevated above the former by a height b_m and the release fluid is bounded at $x = 0$ by an impermeable vertical wall [Fig. 1(a)]. In the second problem, we analyze the flow along a purely horizontal plane with free drainage at $x = 0$ [Fig. 1(b)]. The time after release is denoted by t and we model the depth of the flowing layer, $h(x,t)$, and the depth-averaged velocity, $u(x,t)$. The initial conditions are "lock-release," namely $h = h_0$ for $0 < x < x_0$ and zero otherwise, while the fluid starts from rest, $u = 0$.

We introduce dimensionless variables by scaling horizontal lengths by lock length, x_0 and the fluid depth and boundary elevation by the initial depth of fluid in the lock, h_0. Velocities are scaled by $u_0 = (g'h_0)^{1/2}$ and times by $x_0/(g'h_0)^{1/2}$. The basal drag, τ_b is scaled by $\rho u_0^2(1+\Delta)$. Mixing with the surrounding ambient fluid is neglected and so the reduced gravity does not change from its initial value. In what follows, all variables will be assumed to be dimensionless and on the further

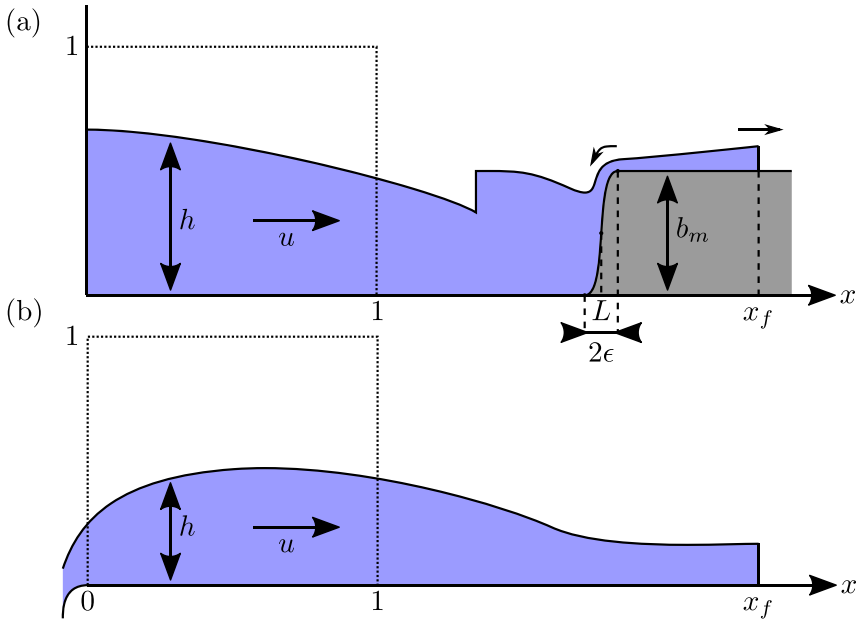

FIG. 1. The configuration of the flow problems and the dimensionless variables: (a) gravity current flow within a topographic depression with step height b_m, located between $x = L - \epsilon$ and $x = L + \epsilon$; and (b) simultaneous spreading and draining along a semi-infinite plane. In (a) and (b) the dotted lines depict the initial lock of fluid of unit dimensionless height and length and the front of the flow is at $x_f(t)$.

assumption that the fluid is in hydrostatic balance so that vertical fluid accelerations are negligible, the governing equations are the nonlinear shallow water equations given by

$$\frac{\partial h}{\partial t} + \frac{\partial}{\partial x}(uh) = 0, \tag{1}$$

$$\frac{\partial}{\partial t}(uh) + \frac{\partial}{\partial x}(u^2 h) + \frac{\partial}{\partial x}\left(\tfrac{1}{2}h^2\right) = -h\frac{\partial b}{\partial x} - \tau_b, \tag{2}$$

In this latter equation we have neglected shear in the velocity field and thus assumed that the momentum shape factor is unity. This assumption is common in gravity current modeling [2], but we note that its inclusion does change the predicted flows somewhat (see, for example, Refs. [25] and [26]). The single layer model (1) and (2) has been recently employed to investigate unsteady reflection [10] and overtopping of obstacles [11] and despite its simplicity yields predictions that are close to experimental measurements of these phenomena. Additionally in (2), we have assumed that the bed gradients are small.

The flow may develop discontinuous solutions ("bores") in which case we impose jump conditions that enforce continuity of mass and momentum fluxes: If the discontinuity is at $x = x_s(t)$ with $c = dx_s/dt$, then

$$[(u - c)h] = 0 \quad \text{and} \quad \left[(u - c)^2 h + \tfrac{1}{2}h^2\right] = 0, \tag{3}$$

where $[\ldots]$ represent the change in value between $x = x_s^-$ and $x = x_s^+$. It is not possible to additionally conserve the flux of energy across these discontinuities; instead bores must dissipate energy [12]. The dissipation arises from the solutions being constructed in the limit of vanishing viscosity: The diffusive processes still play a dominant role in the evolution of energy close to the discontinuity despite being negligible for mass conservation and and momentum balance [27].

At the front of the motion, $x = x_f(t)$, the boundary conditions are [13]

$$\frac{dx_f}{dt} = u(x_f, t) = \mathrm{Fr}\sqrt{h(x_f, t)}, \tag{4}$$

where Fr is the imposed Froude number at the front. We anticipate that the Froude number is a function of the density ratio. From theoretical considerations, Ref. [13] asserts that $\mathrm{Fr} = [2(1 + \Delta)]^{1/2}$, while Ref. [28] determine empirically that $\mathrm{Fr} = 1.2$ for Boussinesq currents ($\Delta \ll 1$).

Our first problem (Sec. III) concerns the flow along a smooth depression; we write

$$b(x) = b_m \, \mathrm{S}\left(\frac{x - L}{\epsilon}\right) \quad \text{where} \quad \mathrm{S}(\hat{x}) = \begin{cases} 1, & 1 \leqslant \hat{x}, \\ 1 - \frac{1}{2}(\hat{x} - 1)^2, & 0 \leqslant \hat{x} \leqslant 1, \\ \frac{1}{2}(\hat{x} + 1)^2, & -1 \leqslant \hat{x} \leqslant 0, \\ 0, & \hat{x} \leqslant -1, \end{cases} \tag{5}$$

where the center of the rise in the topography is at $x = L$, occurring over the interval $L - \epsilon < x < L + \epsilon$, and the amplitude of the step is b_m. The flows are confined by an impermeable wall at the back of the reservoir; this leads to the boundary condition

$$u(0, t) = 0. \tag{6}$$

We compute the volume of fluid that escapes from the topographic depression. With the chosen dimensionless variables, the volume per unit width of fluid that has escaped is given by

$$\mathcal{V}(t) = 1 - \int_0^{L+\epsilon} h \, dx. \tag{7}$$

The second series of problems (Sec. IV) tackle flow along a semi-infinite horizontal plane $b(x) = 0$ with free-draining at the rearward edge. The fluid flow is at least critical at this edge and the boundary condition is given by [9]

$$-u(0, t) \geqslant \sqrt{h(0, t)}. \tag{8}$$

This condition embodies conservation of mass and energy fluxes local to the edge of the domain as the fluid drains. It arises from enforcing supercritical flow ($-u > h^{1/2}$) just outside of the domain ($x = 0^-$) on the slope that the fluid flows down. Thus at the edge of the domain ($x = 0$) the fluid can be supercritical, in which case the inequality of (8) applies. Alternatively the flow must transition from subcritical to supercritical as it drains and be critical at the boundary, in which case equality of (8) is enforced. When the flow is inviscid ($\tau_b = 0$) in this second series of problems, the Froude number, Fr, is the only dimensionless parameter and we will demonstrate the effects of varying its value on the evolution of the flow (Sec. IV). The effects of drag are analyzed in Sec. V.

A. Numerical method

The governing equations are integrated numerically. This is done by rewriting the equations in terms of the numerical variable $\mathcal{Q} = [x_f h, (x_f)^2 \mathcal{U} h]^T$ and rescaled spatial coordinate $\mathcal{X} = x/x_f$, where $\mathcal{U} = u - \mathcal{X} dx_f/dt$, [29]. The algorithm is a finite volume scheme using the central-upwind flux by [30]. The reconstruction applies the minmod slope limiter to $\mathcal{Q}$, which is modified to stabilize shocks as discussed in Ref. [31]. The boundary condition (8) is selected by examination of the cell adjacent to the domain end; if it is subcritical, then criticality is imposed, whereas if it is supercritical, then no algebraic boundary condition is imposed. The system of equations for the boundary values is closed by imposing the characteristic equations for the fields leaving the domain (see Ref. [29, test problem 6.1]). The conditions at the front (4) are implemented similarly. The numerical flux at the boundaries is computed directly from the boundary values. The numerical method is validated by comparison with the exact solution derived below.

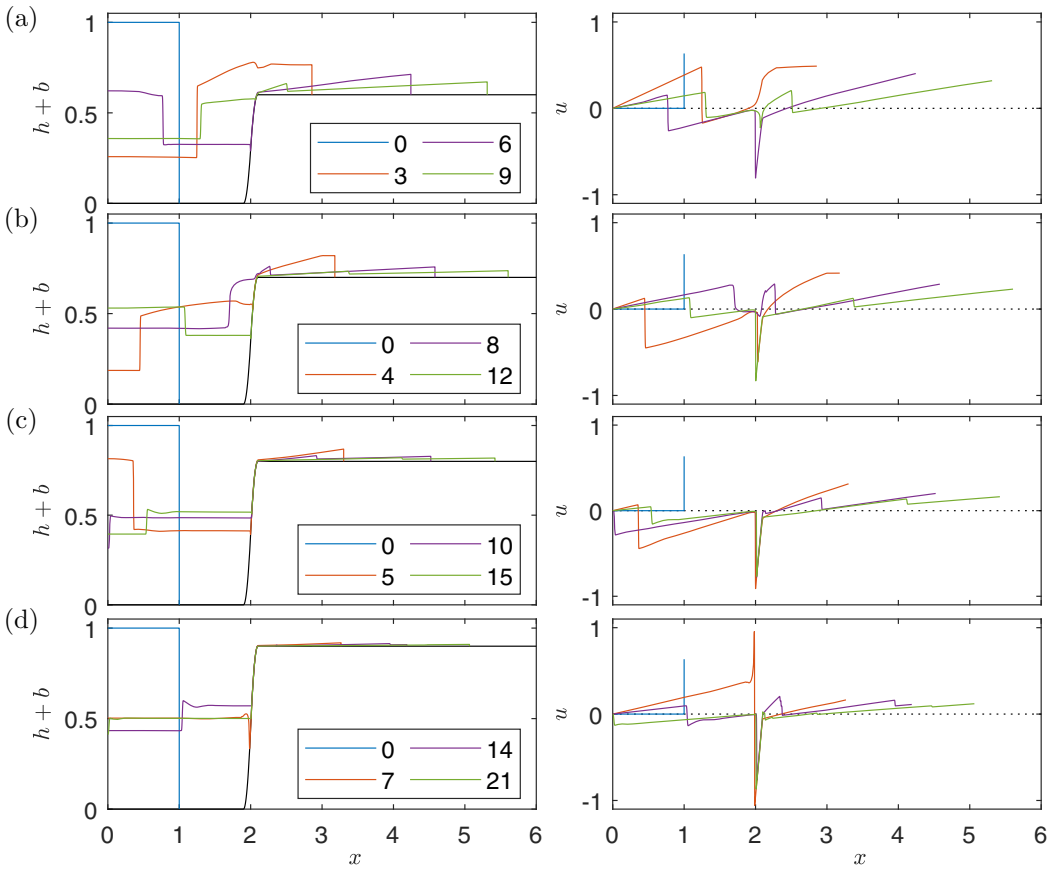

FIG. 2. The elevation of the free surface of the current, $h + b$, and the velocity, u, as functions of distance downstream at various instances of time (shown in each legend) for (a) $b_m = 0.6$, (b) $b_m = 0.7$, (c) $b_m = 0.8$, and (d) $b_m = 0.9$. The elevation of the step, b, is also plotted (black solid line), as is $u = 0$ (black dotted line).

B. Characteristics and hodograph techniques

The inviscid shallow water equations are hyperbolic and admit two characteristic velocities, $dx/dt = u \pm \sqrt{h}$. The flow is termed subcritical when the characteristic velocities are of opposite sign, and supercritical when they are of the same sign. In scenarios where the flow is along a horizontal bed ($\partial b/\partial x = 0$) the characteristic functions, $\alpha = u + 2\sqrt{h}$ and $\beta = u - 2\sqrt{h}$, are respectively conserved along these characteristic curves. Thus the characteristic decomposition of the drag-free governing equations (1) and (2) is given by [12]

$$\frac{d\alpha}{dt} = 0 \quad \text{on} \quad \frac{dx}{dt} = u + \sqrt{h}, \quad \text{and} \quad \frac{d\beta}{dt} = 0 \quad \text{on} \quad \frac{dx}{dt} = u - \sqrt{h}. \tag{9}$$

In this regime it is also useful to employ the hodograph transformation [15], exchanging the dependent and independent variables so that $x = x(\alpha, \beta)$ and $t = t(\alpha, \beta)$. The governing equations are linear under this transformation and solutions may be constructed using a Riemann function and integrating around closed curves in the hodograph plane. Details of this construction and its application to this study are provided in the Appendix. It provides the considerable advantage that the evolution of the flow may be evaluated using quasianalytical techniques; the technique has been used to tackle a number of hydraulic problems modelled by the nonlinear

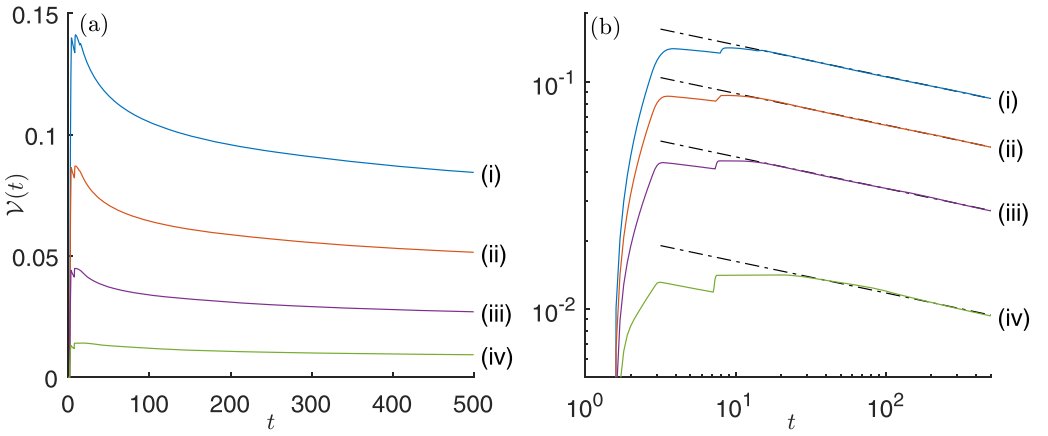

FIG. 3. The dimensionless volume of gravity current fluid escaped from the topographic depression, $\mathcal{V}(t)$, as a function of time on (a) linear and (b) logarithmic axes for (i) $b_m = 0.6$, (ii) $b_m = 0.7$, (iii) $b_m = 0.8$, and (iv) $b_m = 0.9$. The simulations were run with Froude number, $\mathrm{Fr} = 1.2$, while the topography was additionally specified by $L = 2$ and $\epsilon = 0.1$. Also plotted in (b) are power-law relations, $\mathcal{V}(t) \propto t^{-0.139}$, fitted to the data at late times (dashed-dot lines).

shallow water equations. Recent examples include the unsteady drainage from a partially breached lock [16] and the reflection and bore generation of an oncoming current by an initially distant barrier [10]. Key to the use of characteristic methods from lock-release conditions is the identification of regions within which both characteristic functions are constant, or one is constant, or both are varying. We term these regions as uniform, simple wave and complex wave regions, respectively, and denote them by U_i, S_i, and C_i, where i is an integer suffix enumerating each of them.

III. FLOW WITHIN A TOPOGRAPHIC DEPRESSION

We integrate the governing equations (1) and (2) numerically for flow along a surface of elevation given by (5) with $\epsilon = 0.1$, $L = 2$ and $0.6 \leqslant b_m \leqslant 0.9$ and frontal Froude number, $\mathrm{Fr} = 1.2$. Profiles of the elevation of the free-surface, $h + b$, and the velocity, u, are plotted in Fig. 2 at various instants of time for four different heights of the step. These plots show that when the current first reaches the step, some fluid is able to climb up to the raised plateau, whereas some is reflected to form a rearward propagating bore. The fluid on the elevated plateau then propagates away from the step while simultaneous draining back down the step. At the same time the reflected bore is itself reflected from the backwall of the lock and then may surmount the step as a secondary pulse. It is evident from Fig. 2 that as the step height grows, the volume of the fluid that surmounts it diminishes.

The volume of fluid that has escaped from the topographic depression, $\mathcal{V}(t)$, is plotted as a function of time in Fig. 3. In these time series, we see the signature of the dynamics described above. The volume initially increases provided the dimensionless amplitude of the step, $b_m < 2$ [11]. Its magnitude then oscillates as the additional pulses force more fluid up the step to increase the escaped volume (Fig. 3). Bores dissipate energy and so the magnitude of the successive reflections between step and backwall (measured in terms of the relative increase of fluid depth across them) progressively reduces. Eventually they make only a negligible change to the escaped volume. Instead the escaped volume is observed to decrease monotonically with time, due to drainage of fluid back down the step into the topographic depression (Fig. 3). We find the same behavior for each of the simulated cases plotted in Fig. 3 and for other values of the amplitude, b_m, location, L, and threshold parameter, ϵ, used to define the topography, although for larger amplitude steps,

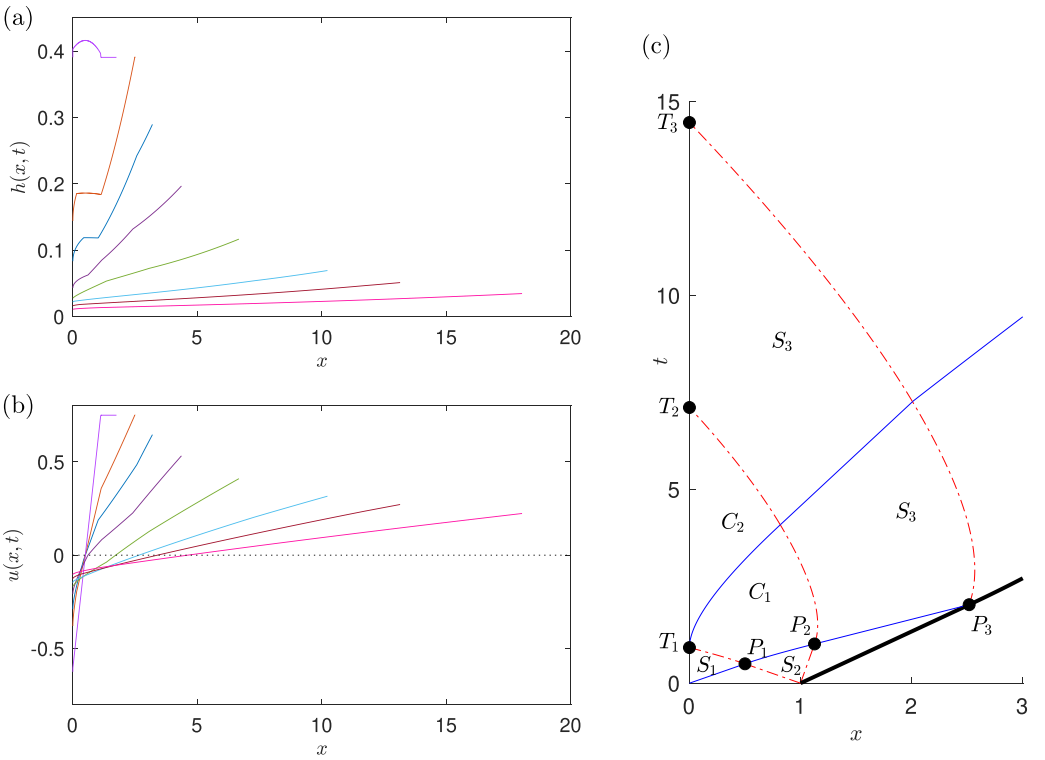

FIG. 4. (a) Depth, $h(x,t)$, and (b) velocity, $u(x,t)$, of the gravity current as functions of distance downstream at $t = 1, 2, 3, 5, 10, 20, 30$, and 50 for $\mathrm{Fr} = 1.2$. (c) The characteristic plane, showing the position of the front, $x_f(t)$ (thick black line) and some α characteristics (solid blue lines) and β characteristics (dot-dashed red lines). The regions of the plane are denoted as simple wave regions (S_1, S_2, S_3) and complex wave regions (C_1, C_2). Also plotted are some key locations in the plane, positions P_1, P_2, and P_3 and the times at which the behavior of the outflow changes (T_1, T_2, T_3).

the secondary overtopping events transport smaller volumes of fluid onto the upper plateau. At late times after release we find that the escaped volume varies as a decaying power law in all cases and that the exponent of this power law is independent of the topographic parameters [Fig. 3(b)]. Instead it depends only on the Froude number at the front of the current and for the simulations plotted in Fig. 3 with $\mathrm{Fr} = 1.2$ exhibit $\mathcal{V} \propto t^{-0.139}$ (see Sec. IV B). Ultimately all of the fluid is found to drain from the step back into the topographic depression and the escaped volume vanishes [$\mathcal{V}(t) \to 0$ as $t \to \infty$]. We find the same behavior for other functions that specify the smooth step (5) (but these are not plotted here) and the same power law for the long-term decay of the escaped volume. This behavior and dependence on the Froude number is examined in the sections that follow, in which we investigate the motion on the upper plateau.

IV. FLOW ALONG AND DRAINING FROM A STEP: INVISCID MOTION

In this section we focus solely on the dynamics of a gravity current which propagates along a semi-infinite horizontal plane, with front condition given by (4), and which drains freely at the rearward edge of the plane (8); this configuration is sketched in Fig. 1(b). To illustrate the behavior, we integrate the governing equations numerically from lock-release conditions for two different values of the frontal Froude number, namely $\mathrm{Fr} = 1.2$ (Fig. 4) and $\mathrm{Fr} = 4$ (Fig. 5). For both simulations we plot profiles of the fluid depth and velocity at various instances of time, alongside the

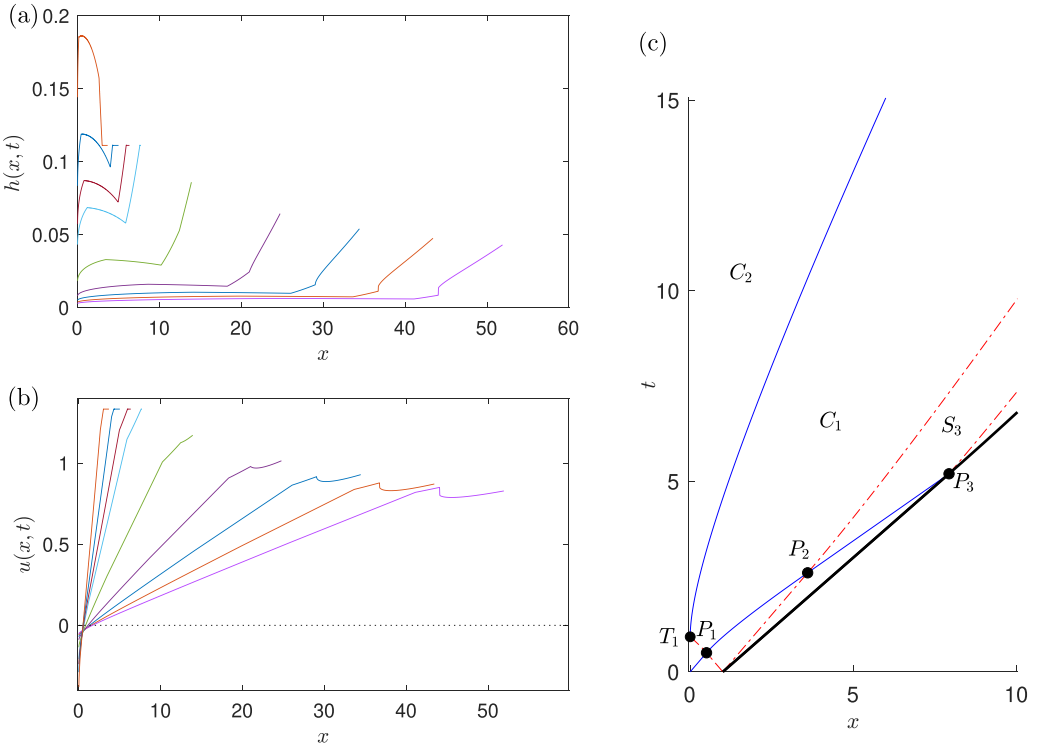

FIG. 5. (a) Depth, $h(x,t)$, and (b) velocity, $u(x,t)$, of the gravity current as functions of distance downstream at $t = 2, 3, 4, 5, 10, 20, 30, 40$, and 50 for $\mathrm{Fr} = 4$. (c) The characteristic plane, showing the position of the front, $x_f(t)$ (thick black line) and some α characteristics (solid blue lines) and β characteristics (dot-dashed red lines). Some of the regions of the plane are labeled as a simple wave regions (S_3) and complex wave regions (C_1, C_2). Also plotted are some key locations in the plane, positions P_1, P_2, and P_3 and the time at which the behavior of the outflow changes (T_1).

characteristic plane, and we extend the simulations to late times after release to capture the volume flux per unit width draining from the plane, $q(t) = u(0,t)h(0,t)$ and the volume of fluid per unit width that remains on the plane,

$$V(t) = 1 - \int_0^t q\, dt. \tag{10}$$

This quantity is analogous to the escaped volume computed in Sec. III.

For $\mathrm{Fr} = 1.2$, we observe that the initially motionless reservoir of fluid slumps into motion, both draining at $x = 0$ and driving a propagating front at $x = x_f(t)$. At very early times, the gravitational collapse at both ends of the current is independent of the other, but soon ($t > 1/2$) they begin to influence each other. This is most easily seen from the characteristic plane plotted in Fig. 4(c). There is a rearward propagating β characteristic from the lock gate ($x = 1$), which first reaches and modifies the outflow at $t = T_1$, and a forward propagating α characteristic from the outflow ($x = 0$) that catches up with the front of the current at a location P_3 in the characteristic plane. These two leading rearward- and forward-propagating curves intersect each other at P_1, which will be shown below to occur at $(x,t) = (\frac{1}{2}, \frac{1}{2})$. On reaching the front at location P_3 in the characteristic plane, this incoming α characteristic is reflected generating a β characteristic (see Fig. 4). Similarly rearward propagating β characteristics are reflected from the outflow to form α characteristics. The first reflection of the rearmost characteristic from the lockgate occurs at location $(x,t) = (0, T_1)$ in

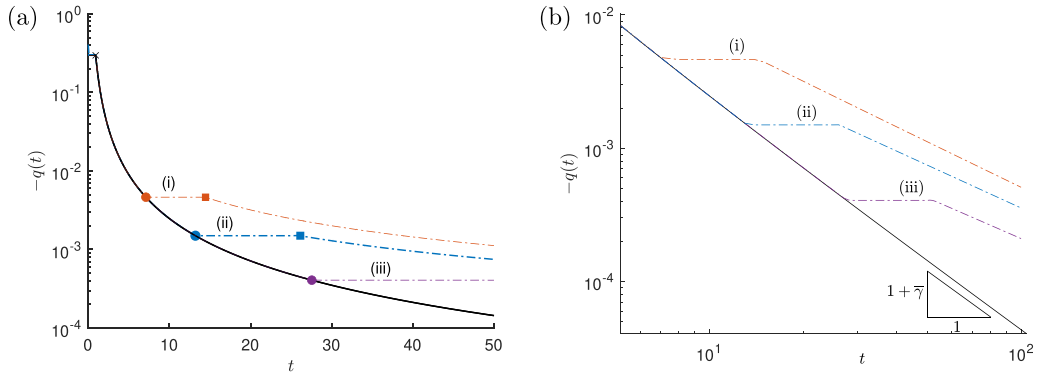

FIG. 6. The drainage flux, $q(t)$, as a function of time, t, on (a) linear and (b) logarithmic axes for (i) Fr $= 1.2$ (red dot-dashed line), (ii) Fr $= \sqrt{2}$ (blue dot-dashed line), and (iii) Fr $= 1.6$ (purple dot-dashed line), along with the universal curve for Fr $\geqslant 2$ (black solid line). Also plotted at the values of q at $t = T_1$ (cross), $t = T_2$ (circle), and $t = T_3$ (square). The first time, T_1, is the same for all values of Fr, but the latter two vary with Fr.

the characteristic plane [Fig. 4(c)]. There follows a pattern of successive reflections similar to that found in nondraining gravity currents [15]. The magnitude of the reflections diminishes and the current approaches a self-similar state at relatively late times.

The motion when Fr $= 4$ shares several of these features (Fig. 5). The initial collapse generates forward propagating α characteristics from $x = 0$ and rearward propagating β characteristics that modify the front propagation and drainage respectively. However, at this value of the frontal Froude number, β characteristics generated by the reflection of forward propagating α characteristics at locations P_3 are not rearward propagating and do not alter the outflow at $x = 0$. At quite late times following the release (for Fr $= 4$, $t = 29.85$, see Sec. IV C), the flow generates an interior shock, which ultimately separates a thin tail of the flow from a much deeper region close to the front. This shock propagates forwards and the ratio of the fluid depth downstream to upstream of the jump continues to grow [Figs. 5(a) and 5(b)].

In Fig. 6 we plot the drainage flux, $q(t)$, for simulations with Fr $= 1.2, \sqrt{2}, 1.6, 2$ and 4 (although the curves for Fr $= 2$ and Fr $= 4$ are identical). We observe that the initial behavior is similar for all of the cases; they follow a universal curve. The drainage flux is constant during some initial period ($t < T_1$) and then decreases. If Fr < 2, then the evolution diverges from the universal curve at some time ($t = T_2$) and its behavior becomes dependent on Fr. In contrast the cases Fr $= 2$ and Fr $= 4$ (and in fact any value of Fr $\geqslant 2$) follow the same temporal dependence of $q(t)$ throughout. At late times the drainage flux follows a power-law relationship with t (see Fig. 6) The exponent is shown to depend on Fr when Fr < 2 and adopts a universal value when Fr $\geqslant 2$; the latter is denoted by $t^{-(1+\overline{\gamma})}$. This dependence is examined theoretically below (Sec. IV B); in what follows we use analytical techniques to reveal the controlling features of these dynamics and to determine quantitatively the long-time behavior.

A. Initial phases of the motion

The reservoir of fluid slumps on release and the initial stages of the motion at each end are unaffected by the other end, each generating a simple wave region between which the fluid remains unchanged from its initial condition. We denote this undisturbed region by U_1, within which $h = 1$ and $u = 0$ (and so $\alpha = -\beta = 2$). In the region adjacent to the outflow ($x = 0$), the solution is a

rarefaction fan of varying α,

$$\sqrt{h} = \begin{cases} (2+y)/3, & y < 1, \\ 1, & 1 \leqslant y, \end{cases} \quad \text{and} \quad u = \begin{cases} -2(1-y)/3, & y < 1, \\ 0, & 1 \leqslant y, \end{cases} \tag{11}$$

where $y \equiv x/t$. This corresponds to a simple wave within the region $S_1 = \{(x,t) : 0 \leqslant y < 1\}$, for which $\beta = -2$ and $2/3 \leqslant \alpha \leqslant 2$, behind the uniform region U_1. Notably the drainage flux per unit width at the outflow is $q(t) = u(0,t)h(0,t) = -\frac{8}{27}$.

Meanwhile, centered at the front of the lock ($x = 1$), we find that

$$\sqrt{h} = \begin{cases} 1, & \tilde{y} \leqslant -1, \\ (2-\tilde{y})/3, & -1 < \tilde{y} \leqslant \tilde{y}_c, \\ (2-\tilde{y}_c)/3, & \tilde{y}_c < \tilde{y} \leqslant \tilde{y}_f, \end{cases} \quad \text{and} \quad u = \begin{cases} 0, & \tilde{y} \leqslant -1, \\ 2(1+\tilde{y})/3, & -1 < \tilde{y} \leqslant \tilde{y}_c, \\ 2(1+\tilde{y}_c)/3, & \tilde{y}_c < \tilde{y} \leqslant \tilde{y}_f, \end{cases} \tag{12}$$

where $\tilde{y} \equiv (x-1)/t$, $\tilde{y}_c = 2(\mathrm{Fr}-1)/(\mathrm{Fr}+2)$, and $\tilde{y}_f = 2\mathrm{Fr}/(\mathrm{Fr}+2)$ [15]. The position of the front is given by $x_f = 1 + \tilde{y}_f t$. This motion corresponds a simple wave within the region, $S_2 = \{(x,t) : -1 \leqslant \tilde{y} \leqslant \tilde{y}_c\}$, for which $\alpha = 2$ and $-2 \leqslant \beta \leqslant \beta_f$, where

$$\beta_f = \frac{2(\mathrm{Fr}-2)}{2+\mathrm{Fr}}. \tag{13}$$

The simple wave region, S_2 is sandwiched between two uniform regions: the undisturbed uniform region U_1 and a region at the front, $U_2 = \{(x,t) : \tilde{y}_c < \tilde{y} < \tilde{y}_f\}$, within which $\alpha = 2$ and $\beta = \beta_f$.

The initial stages of the motion are therefore given by back-to-back rarefaction fans. These two rarefaction fans occur for both $\mathrm{Fr} = 1.2$ and $\mathrm{Fr} = 4$ (see Figs. 4 and 5). We have labeled the simple wave regions S_1 and S_2 in Fig. 4(c) but have omitted this labeling for clarity in Fig. 5(c). The flow structure changes when the lead α characteristic from S_1 intersects the rearmost β characteristic from S_2 at position P_1, which is given by $(x,t) = (1/2, 1/2)$. Thereafter the motion and the characteristic plane are modified.

The drainage flux, $q(t)$, is first changed when the $\beta = -2$ characteristic from P_1 reaches the outflow at $(x,t) = (0, T_1)$ (see Fig. 6). This curve is most conveniently calculated as a parametric function of α and written as $(x_1(\alpha), t_1(\alpha))$. From (9) it satisfies

$$\frac{\partial x_1}{\partial \alpha} = \frac{(\alpha-6)}{4}\frac{\partial t_1}{\partial \alpha}, \tag{14}$$

while each α characteristic within S_1 is a straight line given by

$$x = \tfrac{1}{4}(3\alpha - 2)t, \tag{15}$$

Thus we find that

$$x_1 = \frac{2^{3/2}(3\alpha-2)}{(4+2\alpha)^{3/2}} \quad \text{and} \quad t_1 = \frac{2^{7/2}}{(4+2\alpha)^{3/2}}. \tag{16}$$

This $\beta = -2$ characteristic reaches the outflow when $\alpha = 2/3$ and thus when $t_1 = T_1 \equiv \sqrt{27/32}$. Hence the drainage flux is constant and given by $q(t) = -\frac{8}{27}$ during the interval $0 \leqslant t \leqslant T_1$.

During the next phase of the motion ($t > T_1$), the drainage flux is reduced from its initial value by the arrival of β characteristics from $x = 1$ [see Fig. 4(c) and 5(c)]. They pass through simple wave region S_2 (and $-2 \leqslant \beta \leqslant \beta_f$) and then complex wave regions C_1 and C_2 before reaching the outflow. The analytical task is to calculate the solution in these latter regions.

First we find the boundary to the region S_2, which corresponds to the $\alpha = 2$ characteristic passing through P_1 and continuing to P_2 and P_3 (Figs. 4 and 5). On the segment P_1P_2, we denote this curve parametrically by $(x_2(\beta), t_2(\beta))$ and find that

$$t_2 = \frac{4}{(2-\beta)^{3/2}} \quad \text{and} \quad x_2 = 1 + \tfrac{1}{4}(2+3\beta)t_2, \tag{17}$$

for $-2 \leqslant \beta \leqslant \beta_f$. (These expressions are equivalent to those derived by Hogg [15] up to a factor of $\frac{1}{2}$, which arises for the configuration of the current problem.) The limiting point on this curve, P_2, is given by $(x_2(\beta_f), t_2(\beta_f))$, as plotted in Fig. 4(c). This $\alpha = 2$ characteristic then continues across the uniform region adjacent to the front, U_2, to reach the front at P_3. Within this region, the characteristic is a straight line and P_2 is located at $(x, t) = (1 + 4\mathrm{Fr}\, t_2(\beta_f)/(2 + \mathrm{Fr}), 2t_2(\beta_f))$.

The characteristic curves (x_1, t_1) and (x_2, t_2) provide the boundary data which enable the construction of the solution within the region C_1. Following Ref. [15] and as explained in Appendix, it is straightforward to show that within C_1

$$t(\alpha, \beta) = \tfrac{1}{2}B(2, -2; \alpha, \beta), \tag{18}$$

where $B(a, b; \alpha, \beta)$ is the Riemann function for the hodograph problem (see Appendix). The solution for $x(\alpha, \beta)$ may be calculated by integrating (A1). The region is bounded by the $\alpha = 2/3$ characteristic emanating from $(x, t) = (0, T_1)$ and by the $\beta = \beta_f$ characteristic from P_2 (see Fig. 4). These two characteristic curves are denoted by $(x_3(\beta), t_3(\beta))$ and $(x_4(\alpha), t_4(\alpha))$, respectively, and the time fields are compactly given by

$$t_3(\beta) = \tfrac{1}{2}B\big(2, -2; \tfrac{2}{3}, \beta\big) \quad \text{and} \quad t_4(\alpha) = \tfrac{1}{2}B(2, -2; \alpha, \beta_f), \tag{19}$$

while the spatial fields x_3 and x_4 are readily evaluated using (A1). The final stage in this analysis is to evaluate the solution in C_2, and in particular to find the solution along $x = 0$ in order to evaluate the drainage flux. This construction is more complicated than the previous expressions. We denote the temporal field at the outflow $x = 0$ by $t_w(\alpha) \equiv t(\alpha, -3\alpha)$ and in Appendix and show that $t_w(\alpha)$ satisfies an integral equation given by

$$\begin{aligned} t_w(\alpha) = {} & B(\tfrac{2}{3}, -3\alpha; \alpha, -3\alpha)t_3(-3\alpha) + \int_{-3\alpha}^{-2} \left(\frac{\partial B}{\partial b} + \frac{3B}{2\big(\frac{2}{3} - b\big)} \right) t_3(b)db \\ & + \int_{\alpha}^{2/3} \left(3\frac{\partial B}{\partial b} + \frac{3B}{4a} \right) t_w(a)da. \end{aligned} \tag{20}$$

In the first integral of (20), the Riemann function and its derivatives are evaluated with $a = 2/3$ and $\beta = -3\alpha$, whereas in the second integral $b = -3a$ and $\beta = -3\alpha$. This integral equation is straightforwardly solved numerically by iteration; given an estimate of t_w, we use the right-hand side of (20) to generate the next iterate for t_w. We find a converged solution to within a relative error of 10^{-12} within 30 iterations with run times less than 30s.

The solution, $t_w(\alpha)$, is valid until the $\beta = \beta_f$ characteristic from P_2 intersects with the outflow; this is the curve joining P_2 and $(x, t) = (0, T_3)$ [Fig. 4(c)]. At the outflow, critical conditions correspond to $\alpha = -\beta/3$ and so the solution for t_w is valid for $\alpha_m < \alpha < 2/3$, where

$$\alpha_m = -\frac{\beta_f}{3} = \frac{2(2 - \mathrm{Fr})}{3(2 + \mathrm{Fr})}. \tag{21}$$

Since α must be positive at the outflow (because $u = -\sqrt{h}$ and so $\alpha = \sqrt{h}$), we observe immediately that if $\mathrm{Fr} \geqslant 2$, then no reflected β characteristic from the front reaches the outflow [see Fig. 5(c)]. The drainage is completely determined by the solution (20) which is valid for all $t \geqslant T_1$.

Conversely, if $\mathrm{Fr} < 2$, then we find that $\beta = \beta_f$ characteristic from P_2 intersects the outflow and bounds the region C_2 at $t = T_2 \equiv t_w(\alpha_m)$. Ahead of the regions C_1 and C_2 is a simple wave region, S_3, within which $\beta = \beta_f$ (see Fig. 4). The boundaries of S_3 are the $\beta = \beta_f$ characteristics launched from P_2 and P_3; the former is denoted (x_4, t_4) and defined in (19) and the latter is denoted (x_5, t_5). Since both are $\beta = \beta_f$ characteristics

$$\frac{\partial}{\partial \alpha}(x_5 - x_4) = \frac{1}{4}(\alpha + 3\beta_f)\frac{\partial}{\partial \alpha}(t_5 - t_4), \tag{22}$$

while each α characteristic in S_3 is a straight line, given by

$$x_5 - x_4 = \tfrac{1}{4}(3\alpha + \beta_f)(t_5 - t_4). \tag{23}$$

Thence from (22) and (23) we deduce that

$$t_5(\alpha) = t_4(\alpha) + \frac{4}{(\alpha - \beta_f)^{3/2}}. \tag{24}$$

At the outflow when $t = T_2$, we have $\alpha = \alpha_m$ and $\beta = \beta_f$, thus

$$h(0,t) = \frac{\beta_f^2}{9} \quad \text{and} \quad u(0,t) = \frac{\beta_f}{3}, \tag{25}$$

and so the drainage flux is given by $q = -\alpha_m^3 = (\beta_f/3)^3$. At later times the outflow continues to be from the region S_3 and so $(\alpha, \beta) = (\alpha_m, \beta_f)$ and the drainage flux remains constant for $T_2 \leqslant t \leqslant T_3$, where

$$T_3 = t_5(\alpha_m) = T_2 + \frac{1}{2(\alpha_m)^{3/2}}. \tag{26}$$

The drainage flux, q, and the volume of fluid per unit width that remains within the current, $V(t)$, may be directly evaluated from the results of this subsection. To summarize, we have shown that when $0 < t < T_1$,

$$q = -\frac{8}{27} \quad \text{and} \quad V = 1 - \frac{8t}{27}. \tag{27}$$

For $T_1 < t < T_2$, the drainage flux is implicitly given by $q = -\alpha^3$ and thus

$$V = 1 - \frac{8}{27}T_1 - \int_{T_1}^{t} \alpha^3 dt = 1 - \alpha^3 t_w(\alpha) + \int_{2/3}^{\alpha} 3a^2 t_w(a) da. \tag{28}$$

If $\mathrm{Fr} < 2$, then this expression holds for until $t = T_2$ (which occurs at $\alpha = \alpha_m$). Thereafter there follows a period during which the flux remains constant (25) and so for $T_2 < t < T_3$

$$V(t) = V(T_2) - \alpha_m^3 (t - T_2). \tag{29}$$

At later times ($t > T_3$), the flux varies from its constant value and decreases in magnitude. The volume diminishes also and we find that it vanishes as $t \to \infty$ (see Fig. 7 and Sec. IV B). If, however, $\mathrm{Fr} > 2$, then T_2 is infinite and (28) provides an expression for the volume in the current for all times greater than T_1. In particular we find that $V \to 0.4690$ as $t \to \infty$ and thus all currents with $\mathrm{Fr} > 2$ lose the same volume of fluid through drainage.

We plot these analytical results for the drainage flux, q, along with those determined from the numerical integration of the shallow water equations in Figs. 6 and 7, noting that there is excellent correspondence between the two. In Fig. 6(a) we have marked the time, T_1, at which the drainage flux first changes from its initial value and for $\mathrm{Fr} < 2$ the times T_2 and T_3, which are computed above; in Fig. 7 we have marked only the time T_3. We reiterate that the drainage flux follows a universal curve from which it only diverges if $\mathrm{Fr} < 2$.

B. Late time drainage: Fr < 2

At times $t > T_3$ when $\mathrm{Fr} < 2$, the conditions at the outflow emerge from a series of wave reflections between it and the front of the current. This is akin to the multiple reflections found in shallow water models of lock-release gravity currents [15] or from reservoir drainage [7,16]. While in principle these reflections could be tracked analytically using hodograph techniques, the key observations from the numerical computations are that the drainage persists and that ultimately none of the initially released fluid remains in the domain. At late times, we find that the dynamics adjust to self-similar form in which the exponent linking spatial and temporal scales is itself a

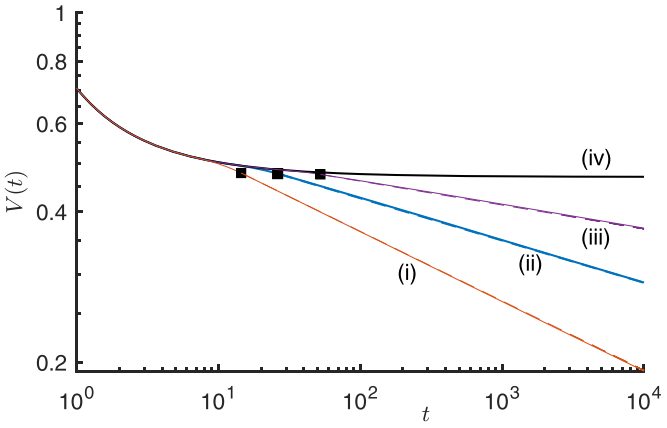

FIG. 7. The volume of fluid per unit width in the flowing current, $V(t)$, as a function of time for (i) Fr $= 1.2$, (ii) Fr $= \sqrt{2}$, (iii) Fr $= 1.6$, and (iv) Fr $= 2$. Also plotted for (i)–(iii) are the volume at $t = T_3$ (squares) and the self-similar solution of the second kind that captures the late time evolution (dashed line).

function of the Froude number at the front and has to be determined as part of the solution. This phase of the motion, therefore, corresponds to a self-similar solution of the second kind (Refs. [17] and [22]).

The self-similar solution is constructed as follows. First we assume that the volume of fluid that remains in the domain varies as a power law in time so that

$$V(t) = \int_0^{x_f(t)} h dx = V_\gamma t^{-\gamma}, \tag{30}$$

where the exponent γ is to be determined as part of the solution and the constant V_γ is fixed by matching the evolution to earlier times.

The volume constraint therefore requires that $hx_f \sim t^{-\gamma}$, while for dynamical balance both at the front and the outflow, $u^2 \sim h$. Thus since $u \sim x_f/t$ for kinematic consistency, we determine the gearing between spatial and temporal coordinates in this self-similar state requires that $x_f \sim t^{(2-\gamma)/3}$ and we seek a self-similar solution of the form

$$h = K^2 t^{-2(1+\gamma)/3} H(\xi), \quad u = K t^{-(1+\gamma)/3} U(\xi), \quad \text{and} \quad x_f = K t^{(2-\gamma)/3}, \tag{31}$$

where $\xi = x/x_f$. The exponent γ, the constant K, and the similarity functions $H(\xi)$ and $U(\xi)$ are determined as part of the solution. We note that if $\gamma = 0$, then the volume does not decay temporally and this formulation recovers the similarity solutions for a constant volume gravity current [32,33]. For the flows analyzed in this study, $\gamma = 0$ is the appropriate value for the late-time dynamics of currents with Fr $\geqslant 2$.

Inserting (31) into (1) and (2), we find the similarity functions must satisfy

$$-\tfrac{2}{3}(1+\gamma)H - \tfrac{1}{3}(2-\gamma)\xi H' + (UH)' = 0, \tag{32}$$

$$-\tfrac{1}{3}(1+\gamma)U - \tfrac{1}{3}(2-\gamma)\xi U' + UU' + H' = 0, \tag{33}$$

where a prime represents differentiation with respect to ξ. The boundary conditions are

$$U = -H^{1/2} \quad \text{at} \quad \xi = 0, \quad \text{and} \quad U = \mathrm{Fr} H^{1/2} = \tfrac{1}{3}(2-\gamma) \quad \text{at} \quad \xi = 1. \tag{34}$$

We numerically integrate (32) and (33) using numerical shooting from the outflow to the front. When $\xi \ll 1$, the similarity functions are given by

$$H = H_0 + U_1 H_0^{1/2} \xi^{1/2} + \ldots, \quad U = -H_0^{1/2} + U_1 \xi^{1/2} + \ldots, \tag{35}$$

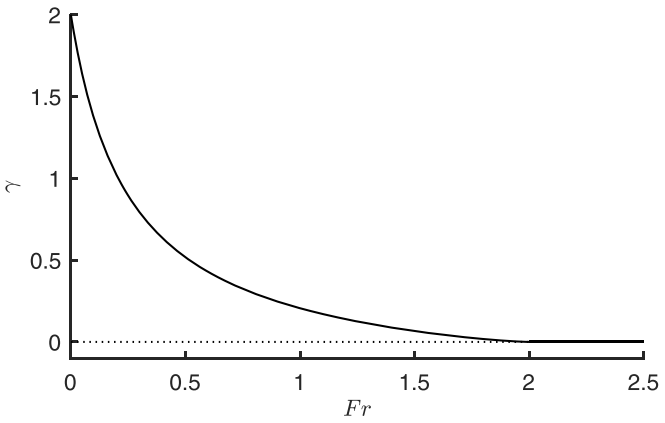

FIG. 8. The self-similar exponent, γ, as a function of the Froude number Fr. Note that $\gamma = 0$ for Fr $\geqslant 2$, indicating that at late times, volume is conserved for these currents.

where $U_1^2 = \frac{2}{9}(\gamma + 1)H_0^{1/2}$. For a chosen value of H_0 and γ, we then integrate numerically from $\xi = \delta \ll 1$ to $\xi = 1$ and iteratively adjust γ until the kinematic boundary condition (34) is satisfied, ensuring that δ is sufficiently small so that the solution is independent of it. The chosen value of H_0 then corresponds to a solution with a particular value of Fr; or conversely, we can adjust H_0 to achieve the required value of Fr. Finally the constant K is determined from (30) and given by

$$K^3 \int_0^1 H d\xi = V_\gamma. \tag{36}$$

where V_γ is still to be determined.

We note, first, that $\gamma = 0$ when Fr $= 2$ and $U(\xi) = 2\sqrt{H(\xi)} = 2\xi/3$. Thus $U(0)H(0) = 0$, so that there is no corresponding drainage flux. This implies that when Fr $= 2$, not all of the released volume drains away and the long-term similarity limit is of a constant volume current propagating such that $x_f \sim t^{2/3}$. When Fr > 2, the rearmost point moves forward in proportion to $t^{2/3}$ and detaches from the outflow; Gratton and Vigo [33] show that for similarity solutions for volume-preserving gravity current of this form are given by

$$U = \frac{2\xi}{3} \quad \text{and} \quad H = \frac{1}{9}\left(\xi^2 + \frac{4}{\mathrm{Fr}^2} - 1\right) \quad \text{for} \quad \xi_b < \xi < 1, \tag{37}$$

where $\xi_b = (1 - 4/\mathrm{Fr}^2)^{-1/2}$ and the constant K follows from the expression of global volume conservation (36), where V_γ is the now constant volume that remains in the detached current. This is the asymptotic state for late times, although as will be shown in the next subsection these currents leave a diminishing, thin upstream tail, which is also in self-similar form.

When Fr < 2 we find positive exponents γ, which implies that the volume of the current ultimately vanishes as $t \to +\infty$. The dependence of γ on Fr is plotted in Fig. 8, and we note that $\gamma \to 2$, as Fr $\to 0$, recovering the self-similar drainage of a lock first analyzed by Momen *et al.* [7] (although this limiting value corresponds to a flow with a stationary front, which is a different flow scenario from that considered in this study). The profiles of the height and velocity fields of the similarity solutions are plotted in Fig. 9 for Fr $\in \{1.2, 1.4, 1.6, 1.8, 2\}$. We note that the height at the outflow and the magnitude of the velocity field monotonically decrease with increasing Froude number at the front Fr, reflecting that the increased front speed is correlated with a redistribution of the fluid mass towards the front of the current. We compare the behavior predicted by these similarity solutions with the numerical integration of the governing equations from the initial conditions by plotting the volume, V, as a function of t (Fig. 7). We note that as with all similarity solutions

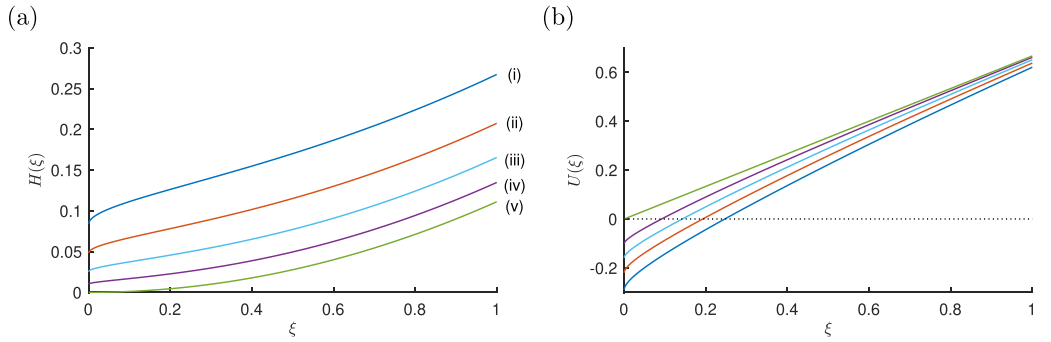

FIG. 9. (a) The self-similar height, $H(\xi)$, and (b) velocity, $U(\xi)$ fields as functions of the similarity variable, ξ, for Fr $\in \{1.2, 1.4, 1.6, 1.8, 2\}$ [labelled (i)–(v), respectively in (a)].

that emerge as $t \gg 1$, it is possible to introduce a temporal offset without changing the solution. The optimal choice of the offset is then a function of the initial conditions. Furthermore for these similarity solutions of the second kind, the constant V_γ must be determined. Here, to compare with the numerical output, we neglect any temporal offset and determine V_γ using $V_\gamma = V(T_3)T_3^{-\gamma}$. This is not necessarily the optimal choice, but we plot the comparison in Fig. 7 and note that it very accurately captures the late-time evolution ($t > T_3$).

C. Late-time drainage: Fr > 2

When Fr > 2 the temporal dependence of the drainage flux follows a universal curve for all times, and at relatively late times after release, the structure of the current is qualitatively different from the counterparts when Fr < 2. First, as is evident from Fig. 5, the flow develops an interior bore at late times after release, which grows in amplitude to separate a thin rearward layer from a much deeper fluid layer close to the front. (Here the amplitude is defined as the ratio of the flows depth downstream to upstream of the jump.) Bore formation is analogous to behavior found in nondraining gravity currents generated by instantaneous lock-release [15]. In addition the flow upstream of the bore evolves towards a self-similar state that feature an anomalous exponent, which cannot be predicted through simple dimensional reasoning; it is another self-similar form of the second kind [17] and is analyzed below.

As for nondraining gravity currents [15], the bore develops on the $\beta = \beta_f$ characteristic that starts from point P_3 in the characteristic plane and is denoted parametrically by (x_5, t_5); see Fig. 5 and (24). The inception of the bore occurs when $\partial t/\partial\beta$ first vanishes at $\beta = \beta_f^+$ and this occurs at a time denoted, t_s. It is straightforward to compute the time and position at which the bore is first created when the forward propagating α characteristics come from the region C_1, because the solution is available in a compact analytical form (18). This restricts our calculation of bore formation to $t_s < t_5(2/3)$. To examine bores at later times, we must include the evolution within region C_2, which entails more complicated expressions that are not presented here.

Following Ref. [15] and after correcting a minor typographical error and introducing the factor of $\frac{1}{2}$ to the time variable (which applies in the current configuration of the problem, as described above), we find that

$$0 = \left.\frac{\partial t}{\partial\beta}\right|_{\beta=\beta_f^+} = \frac{3}{4\beta_f(\alpha-\beta_f)^{5/2}}[2(11\mathrm{Fr}+20)\beta_f - (11\mathrm{Fr}-4)\alpha] + \int_2^\alpha \left(\frac{\partial t_5}{\partial a} + \frac{3t_5}{2(a-\beta_f)}\right)\frac{\partial B}{\partial\beta}(a,\beta_f;\alpha,\beta_f)\,da. \tag{38}$$

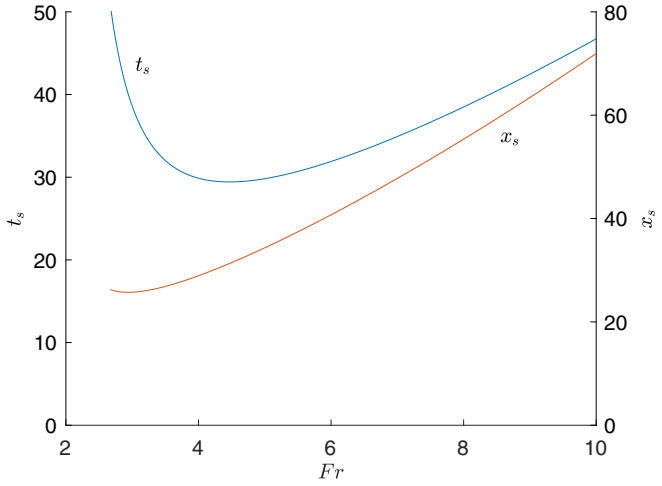

FIG. 10. The time at which a bore forms, t_s (blue) and its position, x_s (red), as functions of the Froude number at the front of the current, Fr.

This algebraic equation for the value of the characteristic variable, α at which $\partial t/\partial\beta$ vanishes, indicates the merger of β characteristics and the onset of a discontinuous solution. In Fig. 10, we plot the time at which the bore form, t_s, and its location, x_s, as functions of Fr, noting that the earliest onset occurs for Fr $= 4.466$ at $t_s = 29.427$. The existence of this local minimum is to be expected, because bores do not form as Fr $\to 2$ (and so $t_s \to \infty$), while as Fr $\to \infty$, the front moves sufficiently fast that it is not caught up by the $\alpha = 2$ characteristic [and given parametrically by (x_2, t_2), see (17)] and so the complex wave region, C_1 remains unbounded. This means that there are no reflections from the front to generate the bore, and so $t_s \to \infty$. For Fr < 2.667, we find that $t_s > t_5(2/3)$ and the onset of the bore is affected by the solution from region C_2 and consequentially the boundary condition at the outflow.

The bore progressively grows in amplitude and at late times the flows develop a thin layer upstream, while downstream there is a thicker frontal region (Figs. 5 and 11). Most of the fluid lies within the latter region. We construct a self-similar solution for the motion upstream of the bore. It shares some features with Sec. IV B, but since we are only seeking an analytical description of the fluid motion within the thin layer upstream of the bore, we cannot pose the expression for global volume evolution (30). Also we cannot enforce the Froude number condition at the front 34(b), because the front is not included within this region.

We seek self-similar forms for the height and velocity fields (31), writing $K = 1$ in this case without loss of generality because we no longer enforce global balance of volume (36) and the remaining equations and boundary conditions are invariant to K. The governing equations are then given by (32) and (33), and the exponent, here denoted as $\overline{\gamma}$, is determined as part of the solution. The governing system is subject to the condition of critical outflow at $\xi = 0$ (34a) and to ensure a bounded solution, the dependent variables must satisfy the following condition at the potentially singular point of (32) and (33):

$$H(\xi_c) = \tfrac{1}{9}(2-\overline{\gamma})^2\xi_c^2 \quad \text{and} \quad U(\xi_c) = \tfrac{2}{3}(2-\overline{\gamma})\xi_c. \tag{39}$$

We integrate the system numerically using the local expansion (35) to step away from the edge of the plane. We integrate until $4H = U^2$, which occurs at $\xi = \xi_c$; we then iteratively adjust the exponent, $\overline{\gamma}$ until $U(\xi_c)/\xi_c = \frac{2}{3}(2-\overline{\gamma})$. In this way we find that $\overline{\gamma} = 0.6974$. Then given a value of $H(0) = H_0$, we may then numerically integrate (32) and (33) to find $H(\xi)$ and $U(\xi)$. As is usual for self-similar solutions of the second kind that are realized asymptotically at late times, the evolution at earlier times before the behavior is accurately predicted by the similarity solution influences the

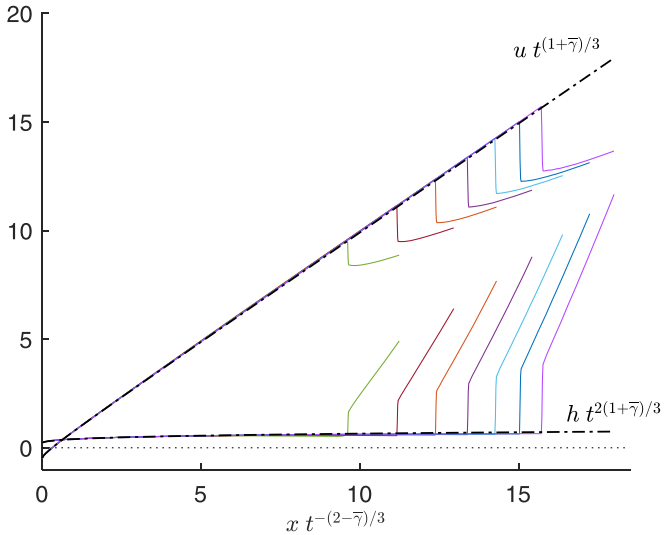

FIG. 11. The rescaled depth and velocity fields as a function of the similarity variable $\xi = xt^{-(2-\overline{\gamma})/3}$ for $\mathrm{Fr} = 4$ and at late times after release $t = 80$, 120, 160, 200, 240, 280, and 320, determined by the numerical integration of the shallow water equations (solid lines). Also plotted are the self-similar forms upstream of the bore (black dot-dashed line).

value of constants that scale the dependent variables—and in this case the value of $H(0) = H_0$ in (35) is determined by matching to the evolution at earlier times. We do this by numerically fitting the outflow flux, $q = -H_0^{3/2}t^{-(\overline{\gamma}+1)}$ (see Fig. 6). This give $H_0 = 0.222$. We then plot the self-similar functions and the numerically determined height and velocity fields for $\mathrm{Fr} = 4$ in Fig. 11. This shows that the upstream evolution is accurately captured by this self-similar form.

V. DRAG-DOMINATED DRAINING

In the previous section we modelled flow along the plane on the assumption that the effects of drag are negligible and found that the flow decelerates and ultimately all the fluid drains from the step. Even though drag may initially be small relative to the streamwise inertia and pressure gradients, it becomes comparable to these processes as the flow slows and thins and then is ultimately non-negligible. In this section we analyze the motion in the drag-dominated regime.

First in Sec. V A, we examine motion when the dimensionless basal drag depends quadratically on the flow velocity, so that the dimensionless drag $\tau_b = C_D|u|u$ and C_D is a constant drag coefficient. Then in Sec. V B we examine the motion when the drag is determined by molecular viscosity and the leading order balance of streamwise momentum is between the divergence of the viscous stresses and the streamwise pressure gradient (e.g., Ref. [34]). In this way we find that $\tau_b = 3\hat{\nu}u/h$, where $\hat{\nu} = \mu/[\rho(1+\Delta)(g'h_0^3)^{1/2}]$ and μ the dimensional dynamic viscosity [18]. These two regimes could in principle be treated via a unified analysis by writing the dimensionless basal shear stress as proportional to $u|u|(uh/\hat{\nu})^{-\lambda}$, where λ is a constant. However, we chose to present the two cases ($\lambda = 0$, 1) separately for clarity and to enable clear connection with previous works in the viscous regime ($\lambda = 1$).

A. Inertial regime: $\tau_b = C_D|u|u$

We assess the dimensionless timescale at which drag becomes comparable with the other terms in the balance of streamwise momentum by using the late-time similarity solution, (31) to assess

their magnitude. In this way we find that

$$h\frac{\partial h}{\partial x} \sim \frac{K^3}{t^{(2+\gamma)}} \quad \text{and} \quad C_D u|u| \sim \frac{C_D K^2}{t^{2(1+\gamma)/3}}. \tag{40}$$

Hence these terms are of the same magnitude when $t \sim t_d \equiv (K/C_D)^{3/(4+\gamma)}$. Thus when $t \ll t_d$ the drag-free model of Sec. IV is the leading order description of the dynamics, but when $t \gg t_d$, the leading-order balance of the streamwise momentum is between the pressure gradient and the drag, and the dimensionless governing equations are given by

$$\frac{\partial h}{\partial t} + \frac{\partial}{\partial x}(uh) = 0 \quad \text{and} \quad h\frac{\partial h}{\partial x} = -C_D u|u|. \tag{41}$$

The boundary conditions in this regime are that the front is marked by vanishing height at a location $x_f(t)$, which also satisfies a kinematic condition:

$$h(x_f, t) = 0 \quad \text{and} \quad \frac{dx_f}{dt} = u(x_f, t). \tag{42}$$

The draining requires that

$$h(0, t) = 0, \tag{43}$$

but that hu is nonvanishing at $x = 0$.

We seek a self-similar solution for the motion on the assumption that the volume within the flowing current is given by

$$\int_0^{x_f} h\, dx = V_\sigma t^{-\sigma}. \tag{44}$$

Then we define

$$h = \left(\frac{C_D V_\sigma^3}{t^{3\sigma+2}}\right)^{1/5} \eta_f^{3/2} H(\eta), \quad u = \left(\frac{V_\sigma^2}{C_D t^{2\sigma+3}}\right)^{1/5} \eta_f U(\eta), \quad \text{and} \quad x_f = \eta_f \left(\frac{V_\sigma^2 t^{-2\sigma+2}}{C_D}\right)^{1/5} \tag{45}$$

and the scaled dependent variable is $\eta = x/x_f$. Substituting into the governing equations gives

$$-\frac{(3\sigma+2)}{5}H - \frac{(2-2\sigma)}{5}\eta H' + (UH)' = 0 \quad \text{and} \quad HH' = -U|U|, \tag{46}$$

where a prime denotes differentiation with respect to η. The boundary conditions are $H(0) = 0$, $H(1) = 0$, and $U(1) = (2-2\sigma)/5$. The constant, η_f, is determined from (44) and given by

$$\eta_f^{5/2} \int_0^1 H\, d\eta = 1. \tag{47}$$

The exponent, σ, is an eigenvalue of the differential system. We note that although σ is not yet determined at this stage, it does not depend on any dimensionless parameters and this solution is therefore a similarity solution of the first kind.

We integrate from $\eta = 1$ and shoot to $\eta = 0$, iteratively varying σ to match the draining condition there. To this end we utilize expansion valid when $|1-\eta| \ll 1$, given by

$$H(\eta) = \frac{4(1-\sigma)}{50^{1/2}}(1-\eta)^{1/2} - \frac{2(3+2\sigma)}{15\,2^{1/2}}(1-\eta)^{3/2} + \ldots, \tag{48}$$

$$U(\eta) = \frac{2(1-\sigma)}{5} - \frac{2(3+2\sigma)}{15}(1-\eta) + \ldots. \tag{49}$$

In this way we find that $\sigma = 0.2678$ and $\eta_f = 0.4801$. The profiles of $H(\eta)$ and $U(\eta)$ are plotted in Fig. 12. (Note that $H \sim \eta^{1/4}$ and $U \sim \eta^{-1/4}$ when $\eta \ll 1$ so that H vanishes and the flux UH is nonvanishing as $\eta \to 0$.) We illustrate the emergence of this drag-dominated regime by numerically integrating the complete dimensionless shallow water equations (1) and (2) with $\tau_b = C_D u|u|$ from

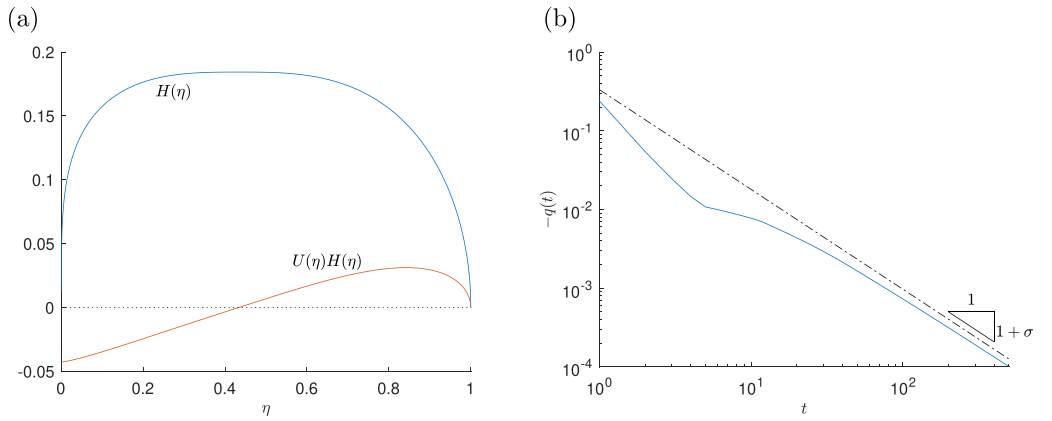

FIG. 12. (a) The similarity solution for the depth of the flow, $H(\eta)$, and flux, $H(\eta)U(\eta)$, as functions of the similarity variable, η, when the drag depends quadratically on the velocity field. (b) The drainage flux as a function of time for Fr $= 1.2$ and $C_D = 0.1$ (blue line). Also plotted is a power-law relation, $t^{-(1+\sigma)}$, with $\sigma = 0.2678$.

lock-release initial conditions. In these simulations we have selected a large value of the drag coefficient ($C_D = 0.1$) in order to realize a relatively early transition from inertial to drag-dominated regimes [$t_d \sim C_D^{-3/(4+\gamma)} = O(10)$]. In Fig. 12(b), we plot the computed drainage flux as a function of time, $q(t)$, noting that at long times it exhibits a power-law dependence. According to the similarity solution (45), $q \sim t^{-(1+\sigma)}$ with $\sigma = 0.2678$ and this is consistent with the numerical data. We have therefore confirmed the emergence of the drag-dominated regime at late times.

B. Viscous regime: $\tau_b = 3\hat{\nu}u/h$

When viscous processes become non-negligible, the drag is given by $3\hat{\nu}u/h$. The regime in which viscous effects are non-negligible could emerge in two ways. The first option is that the flow transitions from a regime in which inertia balances pressure gradients to a regime in which the drag, which depends quadratically on velocity balanced pressure gradients and then to the regime in which viscous drag balances pressure gradients. This latter transition occurs when $C_D u^2 \sim \hat{\nu}u/h$, which using (45) occurs when

$$t \sim t_{v1} = \left(\frac{C_D V}{\hat{\nu}}\right)^{1/(\sigma+1)}. \tag{50}$$

The second possibility is that regime in which the drag depends quadratically on velocity is never dynamically relevant, in which case we estimate the timescale by balancing $h\partial h/\partial x \sim \hat{\nu}u/h$. These are of the same order of magnitude when

$$t \sim t_{v2} = \left(\frac{K^4}{\hat{\nu}}\right)^{3/(7+4\gamma)}. \tag{51}$$

Thus when $t \gg \min(t_{v1}, t_{v2})$ the flow has become viscously controlled.

When the flow has become viscously controlled, the motion is modelled by mass conservation (41a), while the momentum balance (41b) is replaced with

$$h\frac{\partial h}{\partial x} = -3\hat{\nu}\frac{u}{h}. \tag{52}$$

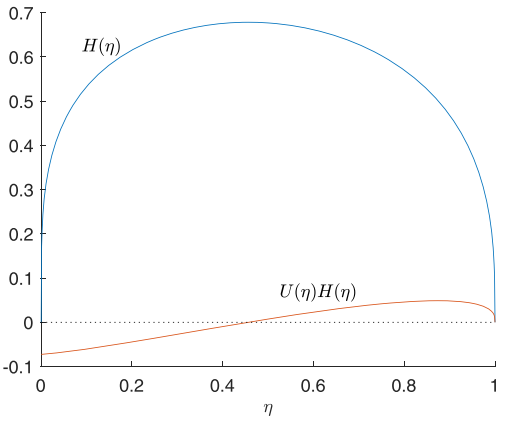

FIG. 13. The similarity solution for the depth of the current, $H(\eta)$, and flux, $H(\eta)U(\eta)$, as functions of the similarity variable, η, when the current is viscously dominated [18,24].

In this case, following Ref. [18], we can show that

$$M = \int_0^{x_f} xh\, dx = \text{const}, \tag{53}$$

where M is known as the dipole moment of the current. It is now possible to compute the similarity solution for the motion which conserves dipole moment, such that $M = M_0$, and this similarity solution of the first kind was presented in Ref. [18]. For completeness, the gearing between spatial and temporal scales may be deduced as follows: The draining flow conserves the dipole and so $x^2 h \sim M_0$, while balance of momentum gives $h^3/x \sim \hat{\nu}x/t$. Thus $x \sim (M_0^3 t/\hat{\nu})^{1/8}$.

The similarity solution is therefore of the form

$$h = \eta_f^{2/3}\left(\frac{\hat{\nu}M_0}{t}\right)^{1/4} H(\eta), \quad u = \eta_f\left(\frac{M_0^3}{\hat{\nu}t^7}\right)^{1/8} U(\eta), \quad \text{and} \quad x_f = \eta_f\left(\frac{M_0^3 t}{\hat{\nu}}\right)^{1/8}, \tag{54}$$

where $\eta = x/x_f$. Its solution is given in Ref. [18] as

$$H = \left(\frac{9\eta^2}{10}(\eta^{-5/4} - 1)\right)^{1/3} \quad \text{and} \quad U = \frac{1}{40}(8\eta - 3\eta^{-1/4}), \tag{55}$$

and the constant, η_f is evaluated from

$$\eta_f^{8/3} \int_0^1 \eta H\, d\eta = 1, \tag{56}$$

which yields $\eta_f = 1.6053$. The profiles of the depth of the fluid and the volume flux are plotted in Fig. 13.

VI. SUMMARY AND DISCUSSION

In this study we have investigated the inviscid motion of gravity currents along a semi-infinite horizontal plane with simultaneous free drainage at the rearward edge. Provided the Froude number at the front, Fr < 2, we have shown that ultimately all of the fluid drains from the step. However, if Fr $\geqslant 2$, then some portion of the current detaches from the edge, leaving a constant volume flowing on the plane. This motion has several intriguing features, notably including a power-law dependencies of the volume of the current and the draining flux on time, which corresponds to a

self-similar phase of the motion. The exponent, γ, that features in the gearing the temporal variable to the spatial variable [see (31)] is dependent on Fr, provided Fr < 2, and this is a self-similar solution of the second kind (see Ref. [17]). Self-similarity of the second-kind also emerges when Fr > 2 for the flow upstream of the bore that separates the thin and progressively draining layer from the bulk of the flow (see Sec. IV C).

We have also presented simulations of gravity currents propagating out of a topographic depression and have shown that these dynamics too exhibit a power-law dependence of the escaped volume on time (Sec. III). For various heights of the confining step, we demonstrated that the volume that escaped varied as a power law, $\mathcal{V}(t) \propto t^{-0.139}$ (Fig. 3). Our analysis of the self-similar phase of simultaneous flow along and draining from the plane allows us to explain this finding (Sec. IV). We showed that the anomalous exponent, $\gamma = 0.139$ for Fr $= 1.2$ (Sec. IV), which is exactly the exponent found in our simulations with topography. Therefore the dynamics of the fluid escaping topographic confinement become dominated by the self-similar balances of simultaneous propagation and draining, and ultimately this explains why the escaped volume vanishes (and the rate at which it does so). It underpins the counterintuitive conclusion that if Fr < 2, then no gravity current fluid can ultimately escape from a topographic depression.

These effects carry over to the dynamics in which drag is no longer negligible (Sec. V). We showed how the long-term motion becomes drag dominated: for viscously controlled motion this reaffirms the role of "dipole" gravity currents [18], and in Sec. V A we computed an analogous result for flow with a drag proportional to the square of the flow speed. Large-scale flows will first exhibit inertially dominated dynamics (Sec. IV) before transitioning to a drag-dominated scenario (Sec. V). For Fr < 2 each regime predicts the ultimate draining of all the dense fluid from the plane, an effect which could by ameliorated if the fluid becomes trapped within small-scale roughness.

Our analysis of the inertial phase of the motion demonstrates further the utility of hodograph calculations for deriving and evaluating quasianalytical results for hydraulic phenomena governed by the nonlinear shallow water equations. We were able to evaluate the draining flux rapidly and accurately using these techniques, validating purely numerically computed solutions, which were then extended to much later times. Moreover the analysis clearly reveals the temporal dependence of the drainage flux, including periods during which it is constant; the potential for flow reflection between the front and the outflow; and the possibility of the onset of bores.

Our results have been derived using numerical and analytical techniques. We are not aware of any experimental studies of these flows in the inertially dominated regime, but note that Ref. [24] report drainage from an edge for viscously dominated flows within a Hele-Shaw cell as a model for flows within porous media. Experimental investigation of flows in the inertial regime would be of considerable interest.

We conclude by noting that it would also be interesting to investigate the topographic confinement of gravity currents driven by the suspension of relatively dense particles. In this scenario, the excess density due to the particles is reduced by progressive settling. We anticipate that currents composed of particles with very low settling velocities will behave quite similarly to the compositional currents analyzed in this study, with most of the escaped volume draining back into the topographic depression. Conversely currents of particles with quite high settling velocities will not propagate sufficiently far from their source to have sufficient kinetic energy to surmount the step; they, too, remain confined. Consequently there must be an intermediate range of settling velocities in which the escaped volume becomes non-negligible, and it would be interesting to deduce its dependence on the properties of the released fluid and geometry of the topography.

ACKNOWLEDGMENTS

E.W.G.S. was supported by the Turbidites Research Group, University of Leeds (funded by AkerBP, CNOOC, ConocoPhillips, Harbour Energy, Murphy Oil, OMV, Oxy, and PetroChina) and by UKRI as a National Fellow in Fluid Dynamics (EP/X028577/1).

APPENDIX: HODOGRAPH TECHNIQUES

1. Problem formulation

By interchanging the independent and dependent variables in (9), it is straightforward to establish evolution equations on characteristic curves $\alpha = \text{const}$ and $\beta = \text{const}$, respectively given by

$$\frac{\partial x}{\partial \beta} = \frac{(3\alpha + \beta)}{4}\frac{\partial t}{\partial \beta} \quad \text{and} \quad \frac{\partial x}{\partial \alpha} = \frac{(\alpha + 3\beta)}{4}\frac{\partial t}{\partial \alpha} \tag{A1}$$

(see, for example, Ref. [15]). Eliminating between them leads to a single linear partial differential equation for $t(\alpha, \beta)$

$$\frac{\partial^2 t}{\partial \alpha \partial \beta} = \frac{3}{2(\alpha - \beta)}\left(\frac{\partial t}{\partial \alpha} - \frac{\partial t}{\partial \beta}\right). \tag{A2}$$

This transformation remains invertible provided the Jacobian, $J = (\alpha - \beta)(\partial t/\partial \alpha)(\partial t/\partial \beta)$ remains nonzero and finite. As derived in Ref. [35] and used by Hogg and coworkers [15,16,36], it is possible to find a Riemann function for (A2), given by

$$B(a, b; \alpha, \beta) = \frac{(a - b)^3}{(a - \beta)^{3/2}(\alpha - b)^{3/2}} F\left(\frac{3}{2}, \frac{3}{2}; 1; \frac{(a - \alpha)(\beta - b)}{(a - \beta)(\alpha - b)}\right), \tag{A3}$$

where F denotes the hypergeometric function. Then Green's theorem leads to the following equation evaluated around a closed curve, $\mathcal{C}$, in the (α, β) plane:

$$\int_{\mathcal{C}} -V \, \mathrm{d}a + U \, \mathrm{d}b = 0, \tag{A4}$$

where

$$U = -\frac{3tB}{2(a - b)} + \frac{B}{2}\frac{\partial t}{\partial b} - \frac{t}{2}\frac{\partial B}{\partial b} \quad V = \frac{3tB}{2(a - b)} + \frac{B}{2}\frac{\partial t}{\partial a} - \frac{t}{2}\frac{\partial B}{\partial a}, \tag{A5}$$

where $B \equiv B(a, b; \alpha, \beta)$ denotes the Riemann function and in which $t \equiv t(a, b)$. This formulation lies at the heart of computing the solution to flows governed by the nonlinear shallow water equations using quasianalytical techniques.

When the outflow is critical at $x = 0$, the boundary condition on the hodograph variables enforces $x = 0$ at $\beta = -3\alpha$. Thus we find that

$$\frac{\partial x}{\partial \alpha} - 3\frac{\partial x}{\partial \beta} = 0 \tag{A6}$$

and using (A1), we deduce

$$\alpha \frac{\partial t}{\partial \alpha} = 0 \quad \text{at} \quad 3\alpha + \beta = 0. \tag{A7}$$

We note that the hodograph transformation remains invertible since this condition is only applied at the boundary of the domain.

At the front the dynamic condition, $u = \mathrm{Fr}\sqrt{h}$ may be written as [15]

$$\alpha(1 + \lambda)\left(\frac{\partial t}{\partial \alpha} + \lambda \frac{\partial t}{\partial \beta}\right) = 0 \quad \text{on} \quad \beta = -\lambda\alpha, \tag{A8}$$

where $\lambda = (2 - \mathrm{Fr})/(2 + \mathrm{Fr})$ and noting that $\beta_f = -2\lambda$ (see Sec. IV A).

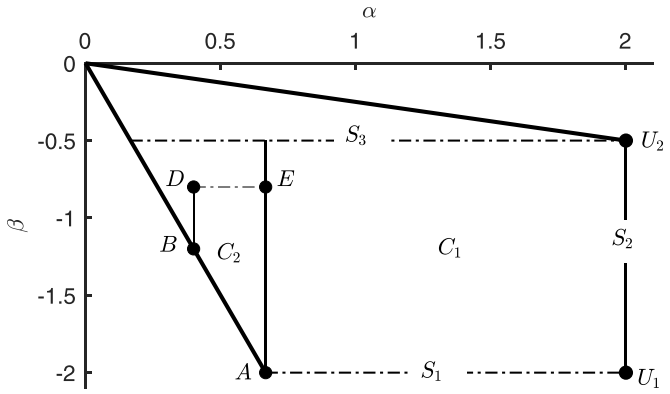

FIG. 14. The hodograph plane for Fr = 1.2, showing regions C_1 and C_2. Characteristics corresponds to lines of constant α (solid) and constant β (dot-dashed). The simple wave regions, S_1, S_2, and S_3, correspond to characteristic lines and uniform regions, and U_1 and U_2 to points in the hodograph plane. The outflow boundary corresponds to the line $\beta = -3\alpha$ and the front to $\beta = (\mathrm{Fr} - 2)\alpha/(\mathrm{Fr} + 2)$ (both plotted with thick black line).The points *ABDE* form a closed curve that is used to construct the solution.

2. Solution in regions C_1 and C_2

After initiation from lock-release conditions and before characteristics are reflected from either the front or the outflow, the flow evolves within a region C_1 within which neither characteristic variables are constant (see Figs. 4 and 5). In the hodograph plane, the region is bounded by the characteristics on which $\alpha = 2$ and $\beta = -2$. These correspond to the forward-propagating α characteristic lying along P_1P_2, for which the solution is parameterically given by $t_2(\beta)$ (17) and the solution along the rearward-propagating β characteristic lying along the curve joining P_1 to $(0, T_1)$ on which $t = t_1(\alpha)$ (16). Integrating (A4) around a rectangular closed curve in the hodograph plane (Fig. 14) joining the four points $(a, b) = (2, -2)$, $(\alpha, -2)$, (α, β), and $(2, \beta)$ leads to the solution

$$t = \tfrac{1}{2}B(2, -2; \alpha, \beta) \tag{A9}$$

and the spatial variable, $x(\alpha, \beta)$ follows from integrating (A1a), subject to the boundary condition that $x(2, \beta) = x_1(\beta)$. This solution is equivalent to that derived in Ref. [15] up to the multiplicative factor of $\frac{1}{2}$ which follows from the configuration of this problem.

The region C_1 is bounded by the $\alpha = 2/3$ characteristic that emanates from the outflow and by the $\beta = \beta_f \equiv -2\lambda$ (see Fig. 4). This former is given parametrically by $(x_3(\beta), t_3(\beta))$ and the latter by $(x_4(\alpha), t_4(\alpha))$ (Fig. 14). The next stage of the analysis is to compute the solution within the region C_2, which lies in between C_1 and the outflow. In the hodograph plane the region C_2 lies in the triangular domain with boundaries $\alpha = 2/3$, $\beta = -3\alpha$ and $\beta = \beta_f$ (Fig. 14).

We may evaluate the solution by integrating around the closed curve *ABDE* with straight-edged segments: A is located at $(a, b) = (2/3, -2)$, B at $(\alpha, -3\alpha)$, D at (α, β), and E at $(2/3, \beta)$. We then integrate (A4) using the boundary data $t(2/3, \beta) = t_3(\beta)$ to find that

$$t(\alpha, \beta) = B\left(\frac{2}{3}, \beta; \alpha, \beta\right)t_3(\beta) + \int_{\beta}^{-2}\left(\frac{\partial B}{\partial b} + \frac{3B}{2\left(\frac{2}{3} - b\right)}\right)t_3(b)\, db + \int_{\alpha}^{2/3}\left(3\frac{\partial B}{\partial b} + \frac{3B}{4a}\right)t_w(a)\, da, \tag{A10}$$

where $t_w(\alpha) = t(\alpha, -3\alpha)$. In the first integral B and its derivatives are evaluated at $a = 2/3$, and in the second they are evaluated at $b = -3a$. Before (A10) can be employed to find $t(\alpha, \beta)$, we must first find the solution along AB [i.e., $t_w(\alpha)$]. To this end we substitute $\beta = -3\alpha$ in (A10) and derive the integral equation given by (20).

[1] J. E. Simpson, *Gravity Currents in the Environment and the Laboratory* (Cambridge University Press, Cambridge, UK, 1997), p. 244
[2] M. Ungarish, *An Introduction to Gravity Currents and Intrusions* (CRC Press, Boca Raton, FL, 2009), p. 489.
[3] P. G. Baines, *Topographic Effects in Stratified Flows* (Cambridge University Press, Cambridge, UK, 1995), p. 477.
[4] E.Gonzalez-Juez and E. Meiburg, Shallow-water analysis of gravity-current flows past isolated obstacles, J. Fluid Mech. **635**, 415 (2009).
[5] T. Tokyay and G. Constantinescu, The effects of a submerged non-erodible triangular obstacle on bottom propagating gravity currents, Phy. Fluids **27**, 056601 (2015).
[6] M. D. Falco, C. Adduce, and M. R. Maggi, Gravity current interacting with a bottom triangular obstacle and implications for entrainment, Adv. Water Resour. **154**, 103967 (2021).
[7] M. Momen, Z. Zheng, E. Bou-Zeid, and H. A. Stone, Inertial gravity currents produced by fluid drainage from an edge, J. Fluid Mech. **827**, 640 (2017).
[8] M. Ungarish, L. Zhu, and H. A. Stone, Inertial gravity current produced by the drainage of a cylindrical reservoir from an outer or inner edge, J. Fluid Mech. **874**, 185 (2019).
[9] E. W. G. Skevington, A. J. Hogg, and M. Ungarish, Development of supercritical motion and internal jumps within lock-release radial currents and draining flows, Phys. Rev. Fluids **6**, 063803 (2021).
[10] A. J. Hogg and E. W. G. Skevington, Dam-break reflection, Q. J. Mech. Appl. Math. **74**, 441 (2021).
[11] E. W. G. Skevington and A. J. Hogg, The unsteady overtopping of barriers by gravity currents and dam-break flows, J. Fluid Mech. **960**, A27 (2023).
[12] G. B. Whitham, *Linear and Nonlinear Waves* (John Wiley & Sons, New York, 1974), p. 636.
[13] T. B. Benjamin, Gravity currents and related phenomena, J. Fluid Mech. **31**, 209 (1968).
[14] M. Ungarish and A. J. Hogg, Models of internal jumps and the fronts of gravity currents: unifying two-layer theories and deriving new results, J. Fluid Mech. **846**, 654 (2018).
[15] A. J. Hogg, Lock-release gravity currents and dam-break flows, J. Fluid Mech. **569**, 61 (2006).
[16] E. W. G. Skevington and A. J. Hogg, Unsteady draining of reservoirs over weirs and through constrictions, J. Fluid Mech. **882**, A9 (2020).
[17] G. I. Barenblatt, *Scaling, Self-similarity and Intermediate Asymptotics* (Cambridge University Press, Cambridge, UK, 1996), p. 386.
[18] J. Gratton and F. Minotti, Self-similar viscous gravity currents: phase-plane formalism, J. Fluid Mech. **210**, 155 (1990).
[19] J. A. Diez and R. Gratton, Self-similar solution of the second kind for a convergent viscous gravity current, Phys Fluids A **4**, 1148 (1992).
[20] D. G. Aronson and J. Graveleau, A self-similar solution to the focusing problem for the porous medium equation, Eur. J. Appl. Math. **4**, 65 (1993).
[21] A. C. Slim and H. E. Huppert, Self-similar solutions of the axisymmetric shallow-water equations governing converging inviscid gravity currents, J. Fluid Mech. **506**, 331 (2004).
[22] C. G. Johnson and A. J. Hogg, Entraining gravity currents, J. Fluid Mech. **731**, 477 (2013).
[23] A. J. Hogg and A. W. Woods, The transition from inertia to bottom-drag-dominated motion of turbulent gravity currents, J. Fluid Mech. **449**, 201 (2001).
[24] S. E. King and A. W. Woods, Dipole solutions for viscous gravity currents: Theory and experiments, J. Fluid Mech. **483**, 91 (2003).
[25] A. J. Hogg and D. Pritchard, The effects of drag on dam-break and other shallow inertial flows, J. Fluid Mech. **501**, 179 (2004).
[26] J. Langham and A. J. Hogg, General linear stability properties of monoclinal shallow waves, Phys. Rev. Fluids **7**, 053902 (2022).
[27] D. Serre, *Systems of Conservation Laws 1: Hyperbolicity, Entropies, Shock Waves* (Cambridge University Press, Cambridge, UK, 1999).
[28] H. E. Huppert and J. E. Simpson, The slumping of gravity currents, J. Fluid Mech. **99**, 785 (1980).

[29] E. W. G. Skevington, A well balanced reconstruction with bounded velocities for the shallow water equations by convex combination, arXiv:2106.11273.
[30] A. Kurganov, S. Noelle, and G. Petrova, Semi-discrete central-upwind schemes for hyperbolic conservation laws and Hamilton-Jacobi equations, SIAM J. Sci. Comput. **23**, 707 (2001).
[31] E. W. G. Skevington, A well balanced reconstruction with bounded velocities and low-oscillation slow shocks for the shallow water equations, arXiv:2106.11256.
[32] D. P. Hoult, Oil spreading on the sea, Annu. Rev. Fluid Mech. **4**, 341 (1972).
[33] J. Gratton and C. Vigo, Self-similar gravity currents with variable inflow revisited: plane currents, J. Fluid Mech. **258**, 77 (1994).
[34] H. E. Huppert, The propagation of two-dimensional and axisymmetric viscous gravity currents over a rigid horizontal surface, J. Fluid Mech. **121**, 43 (1982).
[35] P. R. Garabedian, *Partial Differential Equations* (Chelsea, New York, 1986), p. 672.
[36] A. J. N. Goater and A. J. Hogg, Bounded dam-break flows with tailwaters, J. Fluid Mech. **686**, 160 (2011).